Received: 29 October 2022 | Revised: 11 March 2023 | Accepted: 12 March 2023

DOI: 10.1002/mma.9226

RESEARCH ARTICLE

WILEY

Forward uncertainty quantification in random differential equation systems with delta-impulsive terms: Theoretical study and applications

Vicente J. Bevia | **Juan C. Cortés** | **Rafael J. Villanueva**

Instituto Universitario de Matemática Multidisciplinar, Universitat Politècnica de València, 46022 Valencia, Spain

Correspondence
Vicente J. Bevia, Instituto Universitario de Matemática Multidisciplinar, Universitat Politècnica de València, 46022 Valencia, Spain.
Email: vibees@upv.es

Communicated by: A. Cordero

Funding information
Spanish Ministerio de Economía, Industria y Competitividad (MINECO); Agencia Estatal de Investigación (AEI); Fondo Europeo de Desarrollo Regional (FEDER UE), Grant/Award Number: PID2020-115270GB-I00; Generalitat Valenciana, Grant/Award Number: AICO/2021/302; el Fondo Social Europeo y la Iniciativa de Empleo Juvenil, Grant/Award Number: EDGJID/2021/185; Ayuda a Primeros Proyectos de Investigación, Grant/Award Number: PAID-06-22; Vicerrectorado de Investigación de la Universitat Politécnica de Valéncia (UPV)

This contribution aims at studying a general class of random differential equations with Dirac-delta impulse terms at a finite number of time instants. Our approach directly addresses calculating the so-called first probability density function, from which all the relevant statistical information about the solution, a stochastic process, can be extracted. We combine the Liouville partial differential equation and the random variable transformation method to conduct our study. Finally, all our theoretical findings are illustrated on two stochastic models, widely used in mathematical modeling, for which numerical simulations are carried out.

KEYWORDS

Dirac-delta impulse terms, first probability density function, Liouville–Gibbs equation, random differential equations, random variable transformation technique

MSC CLASSIFICATION

34A34, 34F05, 92D25

1 | INTRODUCTION

Nature is mainly non-stationary; thus, dynamical systems are needed to understand and predict the evolution of natural phenomena, such as cloud evolution in atmospheric physics, population growth in ecology, neuron activation in biology, or even engineering systems, such as a spring–damper system in a train. Most phenomena can be mathematically described as a function evolving smoothly with respect to time, which solves the corresponding differential equation. However, there are cases where the system suddenly changes its state, affecting its dynamics in ways requiring special mathematical tools for its appropriate modeling. This approach leads to formulating differential equations with impulses.

On the other hand, our understanding of nature is also non-deterministic. Dynamical systems used to model natural phenomena often oversimplify the real world. Some variables are discarded to make the model tractable. Other variables are not included because of the unawareness of their effect on the system to be modeled. This source of uncertainty is usually called *epistemic, or structural, uncertainty*. Also, when modeling a specific system, one must take measurements

to calibrate the dynamical system's parameters to the available data. This fact introduces errors in variable values because of the error tolerances in measurement devices and the assumptions made when determining values of variables that are not directly measurable. This source of uncertainty is usually called *aleatoric uncertainty*. See Kiureghian and Ditlevsen [1] and Smith [2] for more information on the different sources of uncertainty.

Consequently, in constructing a dynamical system formulated via differential equations, and modeling real-world phenomena, the uncertainty appearing in the model must be quantified to the greatest extent. One of the most natural and flexible approaches used for the uncertainty quantification (UQ) of continuous dynamical systems is to consider random differential equations (RDEs) [2–6].

In this setting, the deterministic input parameters of the equation (initial/boundary conditions, forcing term, and coefficients) are substituted by their respective random counterpart: random variables and stochastic processes defined on a complete probability space $(\Omega, \mathcal{F}, \mathbb{P})$. Aside from the rigorous calculation of the solution of the RDE, which is a stochastic process, say $\mathbf{X}(t) \equiv \mathbf{X}(t,\omega) = (X_1(t,\omega), \ldots, X_d(t,\omega)), \omega \in \Omega$, many contributions also focus on the computation of its mean and variance functions because of the great statistical information they provide. To calculate, exact or approximately, these statistics for the solution of RDEs, different techniques have been devised, such as generalized polynomial chaos (gPC) [3], Monte Carlo simulations [2], and perturbation methods [4]. However, a more significant goal than computing the first one-dimensional moments of the solution is the determination of the first probability density function (1-PDF) of the solution [4, Ch.3]. Indeed, this deterministic function, say $f_{\mathbf{X}(t)}(\mathbf{x})$ (also denoted by $f(\mathbf{x}, t)$), allows the computation of the expectation ($\mathbb{E}[\,]$) of any measurable transformation, g, of the stochastic process:

$$\mathbb{E}[g(\mathbf{X}(t,\omega)] = \int_{\mathbb{R}^d} g(\mathbf{x}) f_{\mathbf{X}(t)}(\mathbf{x}) \mathrm{d}\mathbf{x}.$$

In the particular case that $g(\mathbf{X}(t,\omega)) = (X_i(t,\omega))^k$, $k = 1, 2, \ldots$, $i = 1, 2, \ldots, d$, one can calculate any one-dimensional statistical moments of the components of the solution,

$$\mathbb{E}[(X_i(t,\omega))^k] = \int_{\mathbb{R}^d} x_i^k f_{\mathbf{X}(t)}(\mathbf{x}) \mathrm{d}\mathbf{x}, \ k = 1, 2, \ldots, \ i = 1, 2, \ldots, d.$$

Taking $k = 1$, one can compute every component of the expectation vector

$$\mathbb{E}[\mathbf{X}(t,\omega)] = (\mathbb{E}[X_1(t,\omega)], \ldots, \mathbb{E}[X_d(t,\omega)]),$$

while taking $g(\mathbf{X}(t,\omega)) = (X_i(t,\omega) - \mathbb{E}[X_i(t,\omega)])^2$, $i = 1, \ldots, d$, one obtains the variance vector

$$\mathbb{V}[\mathbf{X}(t,\omega)] = (\mathbb{V}[X_1(t,\omega)], \ldots, \mathbb{V}[X_d(t,\omega)]).$$

The 1-PDF also permits computing the probability that the solution lies within any region of interest,

$$\mathbb{P}[\{\omega \in \Omega : \mathbf{X}(t,\omega) \in B\}] = \int_B f_{\mathbf{X}(t)}(\mathbf{x}) \mathrm{d}\mathbf{x}, \ B \in \mathcal{B}(\mathbb{R}^d),$$

where $\mathcal{B}(\mathbb{R}^d)$ denotes the Borel σ-algebra of $\mathbb{R}^d$, as well as the computation of confidence regions at a specific level of confidence $1 - \alpha \in (0, 1)$, where $\alpha \in (0, 1)$ is taken as 0.05 to built a 95% confidence interval.

In the setting of ordinary and partial RDEs, the exact or approximate computation of the 1-PDF of the solution has been studied for some relevant class of differential equations such as linear [7], logistic [8], parabolic [9], advection [10], and Korteweg–de Vries [11], including some interesting applications [12, 13]. There have also been advances for RDEs that consider some type of memory in their formulation, as delays or fractional derivatives [14, 15], for example. Although fascinating contributions have been conducted on impulsive stochastic differential equations, many have focused on theoretical aspects, such as stability analysis and control [16–18]. However, the contributions facing the computation of the 1-PDF for impulsive RDEs are still scarce. Recently, some of the authors have studied a class of linear RDEs where the right-hand side involves discontinuities defined by finite impulses (square signals) and infinite impulses (Dirac delta) [19] and [20], respectively. In these papers, the 1-PDF of the solution stochastic process is determined under very general assumptions using the so-called RVT method (an advantageous technique that we shall revise later in the following

Theorem 1.1). The computation of the 1-PDF in these contributions heavily depends on the fact that an explicit solution can be obtained. As the equations studied in Cortés et al. [19, 20] are linear, it is possible to compute their solutions explicitly, and then, the RVT method can be successfully applied. Unfortunately, in the case that the RDE is nonlinear, in general, an explicit solution is not available, and the aforementioned strategy does not work.

Motivated by this fact, in this contribution, we devise a strategy that allows the computation of the 1-PDF for a general class of impulsive RDEs that are particularly relevant in modeling real-world phenomena. To do so, we will combine the two main results we introduce down below, namely, the random variable transformation (RVT) technique and the Liouville partial differential equation (PDE). It must be mentioned that other recent contributions have been developed with the same spirit as the present paper, that is, obtaining the 1-PDF of specific classes of RDEs whose exact solution is not available. In this sense, we here mention the recent contribution by one of the authors [21], where one combines the RVT method with gPC expansions to solve a random SIR-type epidemiological model. Besides combining the RVT technique with another method, namely, Liouville's PDE, in the present paper, we will tackle a different class of RDEs involving delta-impulsive terms continuing the study recently initiated in Bevia et al. [22].

The RVT technique (also known as the probabilistic transformation method). It permits computing the PDF of a random vector obtained by transforming another random vector whose PDF is known. The result can be stated as follows:

Theorem 1.1 ([4, 23])**.** *Let* $\mathbf{X}, \mathbf{Y} : \Omega \to \mathbb{R}^m$ *be two random vectors with PDFs* $f_{\mathbf{X}}$ *and* $f_{\mathbf{Y}}$*, respectively. Assume that there is a one-to-one* C^1 *mapping* $\mathbf{h} : \mathbb{R}^m \to \mathbb{R}^m$*, such that* $\mathbf{X} = \mathbf{h}(\mathbf{Y})$ *with* $\left|\frac{\partial h}{\partial \mathbf{Y}}(\mathbf{y})\right| \neq 0$ *for all* $\mathbf{y}$*. Then, denoting* $\mathbf{h}^{-1}$ *as the inverse mapping of* $\mathbf{h}$*,*

$$f_{\mathbf{X}}(\mathbf{x}) = f_{\mathbf{Y}}(\mathbf{h}^{-1}(\mathbf{x}))\left|\frac{\partial \mathbf{h}^{-1}(\mathbf{x})}{\partial \mathbf{x}}\right|, \tag{1.1}$$

where $\left|\frac{\partial \mathbf{h}^{-1}(\mathbf{x})}{\partial \mathbf{x}}\right|$ *denotes the absolute value of the determinant of the Jacobian matrix.*

The Liouville (also called the continuity) PDE describes the evolution of the 1-PDF of the solution to an RDE.

Theorem 1.2 ([4, 24, 25])**.** *Let* $\mathbf{b}(\cdot, t) : \mathbb{R}^d \to \mathbb{R}^d$ *be a Lipschitz-continuous function for all* $t \in (t_0, \infty)$ *and continuous in* t*. Let* $(\Omega, \mathcal{F}, \mathbb{P})$ *be a complete probability space and* $\mathbf{X}(t) = \mathbf{X}(t, \omega)$*,* $t \geq t_0$*,* $\omega \in \Omega$ *be the stochastic process verifying the following RDE in the almost-surely or mean square sense:*

$$\begin{cases} \frac{\mathrm{d}\mathbf{X}(t)}{\mathrm{d}t} = \mathbf{b}(\mathbf{X}(t), t), \ t > t_0, \\ \mathbf{X}(t_0) = \mathbf{X}_0 \in \mathrm{L}^2(\Omega, \mathbb{R}^d). \end{cases} \tag{1.2}$$

Let $\mathcal{D} \subseteq \mathbb{R}^d$ *be a set such that* $\{\mathbf{X}([t_0, \infty), \omega)\}_{\omega \in \Omega} \subset \overline{\mathcal{D}}$ *almost surely. Then, the 1-PDF of the stochastic process* $\mathbf{X}(t)$*, denoted by* $f = f_{\mathbf{X}(t)}$*, verifies Liouville's PDE:*

$$\begin{cases} \partial_t f(\mathbf{x}, t) + \nabla_{\mathbf{x}} \cdot [\mathbf{b}\, f](\mathbf{x}, t) = 0, \ \mathbf{x} \in \mathcal{D}, \ t > t_0, \\ f(\mathbf{x}, t_0) = f_0(\mathbf{x}), \ x \in \overline{D}, \\ \nabla_{\mathbf{x}} f(\mathbf{x}, t) \cdot \mathbf{n}(\mathbf{x}) = 0, \ x \in \partial D, \ t \geq t_0, \end{cases} \tag{1.3}$$

where f_0 *is the PDF of* $\mathbf{X}_0$*,* $\mathbf{n}$ *is the normal vector of the boundary and* $\nabla_{\mathbf{x}}$ *and* $\nabla_{\mathbf{x}}\cdot$ *denote the gradient and divergence operators, respectively. Also,* $\overline{D} = D \cup \partial D$*.*

Note that the last condition (homogeneous Neumann conditions at the boundary) is only considered wherever ∂D is bounded. Unless specified, we will assume that ∂D is, at least, piecewise C^1 and that f_0 is integrable and C^1 inside its support. Also, note that problem (1.3) could also be set using homogeneous Dirichlet boundary conditions on ∂D instead of homogeneous Neumann boundary conditions. However, using Dirichlet conditions depends on the particular problem to be simulated. There is no computational difference in considering one or another kind of condition.

It must be remarked that the application of Liouville's PDE has as the main limitation that it presumes the 1-PDF is smooth since it must satisfy the PDE itself. This fact limits the application of Liouville's PDE in the cases that the target PDE to be estimated has discontinuities (as the uniform distribution) or is non-differentiable (as the triangular distribution). It is worth noting that this restriction is also shared with another relevant non-parametric method, namely, kernel

density estimation (KDE) [26], that tends to smooth out discontinuities and non-differentiability points of the target density. Nevertheless, it is instructive to point out that some strategies to improve KDE methods for RDEs have been devised [27]. The main disadvantage of the KDE method against Liouville's PDE is that the former requires knowing independent realizations of the solution of the RDE, which is not always available. Although such realizations can be approximated by (numerically) solving the ensemble of deterministic equations that result after applying Monte Carlo to the original RDE, the obtained 1-PDF may severely deteriorate due to the application of all these approximations. Moreover, it must be pointed out the KDE presents a slow convergence rate with the number of realizations [26]. In contrast, when using Liouville's PDE, one directly works with an *exact* equation satisfying the 1-PDF, and advanced numerical techniques to solve this PDE efficiently are available.

As we shall see later, Liouville's PDE will play a key role in our subsequent analysis of a class of RDEs with delta-impulsive terms (see 2.1). However, it must be pointed out that an analogous PDE, often referred to as Fokker–Planck (or forward Kolmogorov) equation, can be formulated when dealing with stochastic differential equations [4, 28]. Liouville's PDE can be derived using different techniques that include the characteristic function [29], Soong [4, Th. 6.2.2], the theory of dynamical systems [30, Th. 8.4], or the principle of preservation of probability [31]. In a recent contribution, one derives Liouville's PDE for the first-order homogeneous semilinear random PDE in a brilliant way, which includes the linear advection equation with random coefficients [32]. In the setting of RDEs, Liouville's PDE has been applied to a variety of problems, such as constructing ensemble approximations for constrained random systems [33], the prediction of forecast skill, and atmospheric predictability [34–36], and to study the motion of a body in a central force field with the theory of satellites [37], just to cite a few contributions. Finally, it is worthy to remark that Liouville's PDE is stated for differential equations whose derivative has an entire order, but Tarasov [38] deduces a Liouville equation for the case of fractional derivatives.

This contribution is organized as follows: Section 2 is divided into three parts. In Section 2.1, we will first present the class of RDEs considered in the contribution. Then, we will build the pathwise solution to the corresponding problem. In Section 2.2, we will use the information gathered about the pathwise solution and Theorems 1.1 and 1.2, stated above to describe the evolution (or forward uncertainty propagation) of the 1-PDF of the solution stochastic process. This will be done by splitting the analysis into two parts, first between impulses (see Section 2.2.1) and, secondly, at the impulses (see Section 2.2.2). In both cases, we obtain semi-explicit (in terms of multidimensional integrals) expressions for the 1-PDF of the solution that can be represented via an expectation. In Section 3, we will give a brief overview of the computational techniques that will be required in the following Section 4, where we will simulate the evolution of a prescribed PDF according to the dynamics of relevant RDEs with impulses that appear in different mathematical models involving uncertainties. Finally, conclusions are drawn in the last section.

2 | THEORY

This section will deal with the theoretical probabilistic analysis of the following class of impulsive random initial value problems (IVPs):

$$\begin{cases} \frac{\mathrm{d}\mathbf{X}(t,\omega)}{\mathrm{d}t} = \mathbf{g}(\mathbf{X}(t,\omega),t,\mathbf{A}(\omega)) - \sum_{k=1}^{N} \mathbf{\Gamma}_k(\omega)\delta(t-t_k),\ t > t_0, \\ \mathbf{X}(t_0,\omega) = \mathbf{X}_0(\omega). \end{cases} \tag{2.1}$$

Here, $t_0 > 0$ denotes the initial time of the system, $\mathbf{X}_0(\omega)$, $\mathbf{A}(\omega) := (A_1(\omega), \ldots, A_m(\omega))$ and $\{\mathbf{\Gamma}_k(\omega) = (\Gamma_k^1(\omega), \ldots, \Gamma_k^d(\omega))\}_{k=1}^N$ are assumed to be pairwise independent absolutely continuous random vectors whose components are random variables defined on the Hilbert space $\mathrm{L}^2(\Omega,\mathbb{R})$, that is, real-valued random variables with finite variance. $(\Omega,\mathcal{F},\mathbb{P})$ denotes a complete probability space [39]; $\delta(t-t_k)$ stands for the Dirac-delta function [40] acting at the prefixed time instants $t = t_k$, $k = 1, \ldots, N$ and $\mathbf{g}$ is known as the *(vector) field function* satisfying certain conditions that will be specified later. Finally, $\mathbf{X}(t,\omega)$ denotes the solution of the random IVP (2.1), which is a stochastic process. For simplification in the notation, the ω-dependence will be hidden in the notation when convenient.

Observe that we set the impulse terms with the negative sign because, in most practical cases, one is often interested in the instantaneous change of the system's state in a way that is opposite to its natural dynamics.

Clearly, the solution of the random IVP (2.1) has some dependence on the sample realizations of the parameter random vector $\mathbf{A}(\omega)$. In order to guarantee the existence and uniqueness of solution in the sample/pathwise sense, that is, for $\mathbb{P}-$a.e (almost everywhere) realization of $\mathbf{A}(\omega), \omega \in \Omega$ (see Soong [4, Appendix I]), one must impose some classical regularity assumptions on the trajectories of $\mathbf{g}$ such as the ones formulated by the Picard–Lindelöf or Cauchy–Peano

theorems [41, 42]. In this manner, one can guarantee the existence and/or uniqueness of solutions for the random IVP (2.1) between the impulses $t = t_k$ generated by the Dirac-delta function $\delta(t - t_k)$. For example, assuming that the event $E = E_1 \cap E_2$, where $E_1 = \{\omega \in \Omega : g(\cdot, t, \mathbf{A}(\omega))$ is Lipschitz in $\mathbb{R}$ uniformly in $t\}$ and $E_2 = \{\omega \in \Omega : g(x, \cdot, \mathbf{A}(\omega))$ is continuous in $[t_0, \infty)$ for all $x \in \mathbb{R}\}$, has probability 1, that is, $\mathbb{P}[E] = 1$, one can guarantee the existence of a global solution, that is, well-defined, between the impulses sequence $\{t_k\}_{k=1}^N$. Further specialized results about the existence and uniqueness of solution for IVP of type (2.1), with $\omega \in \Omega$ fixed, can be found, for instance, in Agarwal and Lakshmikantham [43]. In summarizing, a priori, we cannot guarantee the existence of a solution or its uniqueness. However, as previously indicated, some regularity assumptions are sufficient for assuring each sample trajectory's global existence. Furthermore, if a solution $\mathbf{X}(t)$ exists, it must be "well-behaved" between the impulse times $\{t_k\}_{k=1}^N$, that is, differentiability of the solution between impulse times and the existence of finite limits at the left and right of each impulse time.

2.1 | Pathwise (weak) solution

We will build a pathwise solution for the random IVP (2.1) considering the previous paragraphs' comments. Let us fix $\omega \in \tilde{\Omega}$ and compute the deterministic Laplace transform [44] to the corresponding IVP (2.1). Denoting $\lambda(s) = \mathcal{L}[\mathbf{X}(\cdot, \omega)](s)$, $\mathbf{x}_0 = \mathbf{X}_0(\omega)$, $\mathbf{a} = \mathbf{A}(\omega)$ and, momentarily, dropping the ω notation, we obtain

$$s\lambda(s) - \mathbf{x}_0 = \mathcal{L}[\mathbf{g}(\mathbf{X}(\cdot), \cdot, \mathbf{a})](s) - \sum_{k=1}^{N} \mathbf{\Gamma}_k \mathrm{e}^{-st_k},$$

so

$$\lambda(s) = \frac{1}{s}\mathbf{x}_0 + \frac{1}{s}\mathcal{L}[\mathbf{g}(\mathbf{X}(\cdot), \cdot, \mathbf{a})](s) - \sum_{k=1}^{N} \mathbf{\Gamma}_k \frac{\mathrm{e}^{-st_k}}{s}. \tag{2.2}$$

Computing the inverse Laplace transform of (2.2) gives

$$\mathbf{X}(t) = \mathbf{x}_0 + \int_{t_0}^{t} \mathbf{g}(\mathbf{X}(s), s, \mathbf{a})\mathrm{d}s - \sum_{k=1}^{N} \mathbf{\Gamma}_k \mathrm{H}(t - t_k), \tag{2.3}$$

where $\mathrm{H}(\cdot)$ is the Heaviside function, defined as

$$\mathrm{H}(x) = \begin{cases} 1 \; x \geq 0, \\ 0 \; x < 0. \end{cases} \tag{2.4}$$

Notice that expression (2.3) is the integral form of Equation (2.1), where $\delta(\cdot)$ acts as a measure [45]. Substituting $t = t_1$ and taking into account (2.3) yield

$$\mathbf{X}(t_1) = \mathbf{x}_0 + \int_{t_0}^{t_1} \mathbf{g}(\mathbf{X}(s), s, \mathbf{a})\mathrm{d}s - \mathbf{\Gamma}_1 = \lim_{t \to t_1^-} \mathbf{X}(t) - \mathbf{\Gamma}_1 \; := \mathbf{X}(t_1^-) - \mathbf{\Gamma}_1. \tag{2.5}$$

Now, let us see what happens after the impulse. From (2.3) and the previous relation for $\mathbf{X}(t_1)$, we can compute the jump induced in the paths by the impulse term

$$\mathbf{X}(t_1^+) - \mathbf{X}(t_1^-) = \int_{t_1^-}^{t_1^+} \mathbf{g}(\mathbf{X}(s), s, \mathbf{a})\mathrm{d}s - \mathbf{\Gamma}_1.$$

The integral term in the previous equation is clearly the **0** vector:

$$\begin{aligned}\left\|\int_{t_1^-}^{t_1^+}\mathbf{g}(\mathbf{X}(s),s,\mathbf{a})\mathrm{d}s\right\| &\leq \lim_{\varepsilon\to 0}\left(\int_{t_1-\varepsilon}^{t_1}\|\mathbf{g}(\mathbf{X}(s),s,\mathbf{a})\|\mathrm{d}s+\int_{t_1}^{t_1+\varepsilon}\|\mathbf{g}(\mathbf{X}(s),s,\mathbf{a})\|\mathrm{d}s\right)\\ &\leq \lim_{\varepsilon\to 0}\left(\sup_{t\in[t_1-\varepsilon,t_1)}\|\mathbf{g}(\mathbf{X}(t),t,\mathbf{a})\|\varepsilon+\sup_{t\in(t_1,t_1+\varepsilon]}\|\mathbf{g}(\mathbf{X}(t),t,\mathbf{a})\|\varepsilon\right)\\ &=0,\end{aligned}$$

because both supremum terms are finite due to the regular behavior of the solution between the impulse times. Summarizing, we have the following relations:

$$\mathbf{X}(t_1^+)-\mathbf{X}(t_1^-)=-\mathbf{\Gamma}_1 \iff \mathbf{X}(t_1^+)=\mathbf{X}(t_1^-)-\mathbf{\Gamma}_1=\mathbf{X}(t_1). \tag{2.6}$$

The general solution (2.3) is right-continuous at the first impulse. Furthermore, notice that because of the definition of the Heaviside function (2.4), the equality obtained at (2.6) shows that right-continuity at impulse times will be verified by solutions of Equation (2.1). Recovering the ω-notation, the previous identity is stated as

$$\mathbf{X}(t_1,\omega)=\mathbf{X}(t_1^+,\omega)=\mathbf{X}(t_1^-,\omega)-\mathbf{\Gamma}_1(\omega), \tag{2.7}$$

which shows that, for every sample $\omega\in\tilde{\Omega}$, the paths are right-continuous at $t=t_1$. We can follow the same procedure for the following impulse times. For example, for all $t\in[t_1,t_2]$, the solution process is given by

$$\mathbf{X}(t)=\mathbf{x}_0+\int_{t_0}^{t}\mathbf{g}(\mathbf{X}(s),s,\mathbf{a})\mathrm{d}s-\mathbf{\Gamma}_1-\mathbf{\Gamma}_2\mathrm{H}(t-t_2). \tag{2.8}$$

Now, by using (2.3), we see that, at time $t=t_2$, (2.8) can be written as

$$\mathbf{X}(t_2)=\mathbf{X}(t_1)+\int_{t_1}^{t_2}\mathbf{g}(\mathbf{X}(s),s,\mathbf{a})\mathrm{d}s-\mathbf{\Gamma}_2,$$

which yields

$$\mathbf{X}(t_2)=\mathbf{X}(t_1)+\int_{t_1}^{t_2}\mathbf{g}(\mathbf{X}(s),s,\mathbf{a})\mathrm{d}s-\mathbf{\Gamma}_2=\lim_{t\to t_2^-}\mathbf{X}(t)-\mathbf{\Gamma}_2 :=\mathbf{X}(t_2^-)-\mathbf{\Gamma}_2.$$

Following the same reasoning we used to obtain relation (2.6), the value after the impulse will be

$$\mathbf{X}(t_2^+)-\mathbf{X}(t_2^-)=-\mathbf{\Gamma}_2 \iff \mathbf{X}(t_2^+)=\mathbf{X}(t_2^-)-\mathbf{\Gamma}_2.$$

The steps followed for analyzing the first and second impulse times can be easily generalized for any finite number of impulse times. Particularly, at a given impulse time t_k, and recovering the ω-notation, one gets

$$\mathbf{X}(t_k^+,\omega)=\mathbf{X}(t_k,\omega)=\mathbf{X}(t_k^-,\omega)-\mathbf{\Gamma}_k(\omega), \tag{2.9}$$

for all $k=1,\ldots,N$.

Summarizing, we have constructed a right-continuous pathwise solution of the random IVP (2.1), given by

$$\mathbf{X}(t,\omega)=\mathbf{X}_0(\omega)+\int_{t_0}^{t}\mathbf{g}(\mathbf{X}(s,\omega),s,\mathbf{A}(\omega))\mathrm{d}s-\sum_{k=1}^{N}\mathbf{\Gamma}_k(\omega)\mathrm{H}(t-t_k),\ t\geq t_0, \tag{2.10}$$

$$\mathbf{X}(t_k,\omega)=\mathbf{X}(t_k^-,\omega)-\mathbf{\Gamma}_k(\omega)=\mathbf{X}(t_k^+,\omega),\ k=1,\ldots,N,\ \omega\in\tilde{\Omega}. \tag{2.11}$$

2.2 | Probability density function evolution

We consider two main approaches to studying the evolution of the 1-PDF of the solution to an RDE. On the one hand, the Liouville equation shows that the evolution of the PDF is a conservation law [46] where the quantity to be conserved is the total probability of the system and the flow function is defined at the right-hand side of the corresponding RDE (Theorem 1.2, see Soong [4, Ch. 6]). On the other hand, the RVT theorem gives a relation between the respective PDFs of two random vectors related via one-to-one mapping (recall Theorem 1.1). We will now show how we can take advantage of these two results to completely describe the PDF evolution.

2.2.1 | Evolution between impulse times

As noted throughout the previous subsection, the flow between the impulse times is assumed to verify some conditions equivalent to those of the Liouville equation theorem. Now, we will see a special form of the Liouville equation where the dynamical behavior (mainly transport and rescaling) of the PDF can be easily identified. Let us consider the same notation as in Theorem (1.2). Let $\mathbf{a}$ be a generic but fixed realization of the random parameter vector $\mathbf{A}$. If the field function $\mathbf{b}(\cdot, t, \mathbf{a}) \in C^1(\mathcal{D})$ for all $t > t_0$ and for any $\mathbf{a}$, (1.3) can be written as

$$\partial_t f(\mathbf{x}, t \,|\, \mathbf{a}) + \underbrace{\mathbf{b}(\mathbf{x}, t, \mathbf{a}) \cdot \nabla_{\mathbf{x}} f(\mathbf{x}, t \,|\, \mathbf{a})}_{\text{Transport}} = \underbrace{-f(\mathbf{x}, t \,|\, \mathbf{a}) \nabla_{\mathbf{x}} \cdot \mathbf{b}(\mathbf{x}, t, \mathbf{a})}_{\text{Rescaling}}, \ \mathbf{x} \in \mathcal{D}, \ t > t_0, \tag{2.12}$$

and its solution can be analyzed through its characteristic equations [24, 46, 47]. These curves describe the time evolution of a particle, say $\Phi(t) = (\phi_1, \ldots, \phi_d) \in \mathbb{R}^d$, and the value of the desired PDE solution at that particle's position. These equations form a system of ODEs, which are given by

$$\begin{aligned} \frac{\mathrm{d}}{\mathrm{d}t}\Phi(t) &= \mathbf{b}(\Phi(t), t, \mathbf{a}), \qquad \Phi(0) = \mathbf{x}_0, \\ \frac{\mathrm{d}}{\mathrm{d}t} f(\Phi(t), t \,|\, \mathbf{a}) &= -f(\Phi(t), t \,|\, \mathbf{a}) \nabla_{\mathbf{x}} \cdot \mathbf{b}(\Phi(t), t, \mathbf{a}), \ f(\Phi(0), 0 \,|\, \mathbf{a}) = f_0(\mathbf{x}_0), \end{aligned} \tag{2.13}$$

where $\mathbf{x}_0$ is a generic point in $\mathcal{D}$, which represents the initial position of the particle to be simulated. The first equation defines the time evolution of the particle's position, whereas the last equation in (2.13) defines the evolution of the PDF value in the considered particle. Before solving this system of equations, note that the field function $\mathbf{b}(\cdot, t, \cdot) = \mathbf{g}(\cdot, t, \cdot)$ for all times between impulses; that is, $t \in \cup_{k=1}^{N}(t_{k-1}, t_k)$.

Now, the characteristic curves, which form the solution of the characteristic equations (2.13), are defined by

$$\Phi(t; \mathbf{x}_0, \mathbf{a}) = \mathbf{x}_0 + \int_{t_0}^{t} \mathbf{g}(\Phi(s; \mathbf{x}_0, \mathbf{a}), s, \mathbf{a}) \mathrm{d}s, \ t \geq t_0, \tag{2.14}$$

$$f(\Phi(t; \mathbf{x}_0, \mathbf{a}), t \,|\, \mathbf{a}) = f_0(\mathbf{x}_0) \exp\left(- \int_{t_0}^{t} \nabla_{\mathbf{x}} \cdot \mathbf{g}(\Phi(s; \mathbf{x}_0, \mathbf{a}), s, \mathbf{a}) \mathrm{d}s \right), \ t \geq t_0, \tag{2.15}$$

where $\Phi(t; \mathbf{x}_0, \mathbf{a})$ denotes the characteristic curve at time t, starting at $\mathbf{x}_0$, with parameter values $\mathbf{a}$.

As it can be seen, the first ODE in (2.13) and its corresponding solution (2.14) are the deterministic version of the random IVP (2.1) between impulses, solved for random samples $\mathbf{x}_0$ and $\mathbf{a}$ of the random initial condition $\mathbf{X}_0(\omega)$ and random parameter vector $\mathbf{A}(\omega)$, respectively, with $\omega \in \tilde{\Omega}$. The second equation in (2.13) and its solution (2.15) describe the change in the value of the PDF in time at the sample path $\Phi(t; \mathbf{x}_0, \mathbf{a})$.

It is well known that the flow function of an ODE with a "sufficiently regular" vector field (e.g., Lipschitz in space, continuous in time) is differentiable. As a simple consequence of the inverse function theorem, wherever the vector field is non-zero, and the flow function has continuous derivatives, one can define its inverse function, which will be differentiable (see Hörmander [48, Th. 1.1.7] for more details). Mathematically, it is a differentiable function $\Psi(t; \mathbf{x}, \mathbf{a})$ such that $\Phi(t; \Psi(t; \mathbf{x}, \mathbf{a}), \mathbf{a}) = \mathbf{x}$. This function is called the *inverse flow* function. See Figure 1 for a graphical representation of both functions.

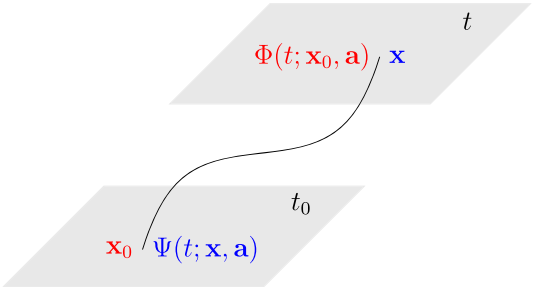

FIGURE 1 The flow function (red) gives the position $\mathbf{x}$ at time t of the characteristic curve starting at $\mathbf{x}_0$. The inverse flow function (blue) gives the point where the curve must start, $\mathbf{x}_0$, so that it is located at $\mathbf{x}$ at time t. [Colour figure can be viewed at wileyonlinelibrary.com]

With the notion of the inverse flow in mind, we can now write (2.15) as

$$f(\mathbf{x}, t\,|\,\mathbf{a}) = f_0(\Psi(t;\mathbf{x},\mathbf{a}))\exp\left(-\int_{t_0}^{t}\nabla_{\mathbf{x}}\cdot\mathbf{g}(\Phi(s;\Psi(t;\mathbf{x},\mathbf{a}),\mathbf{a}),s,\mathbf{a})\mathrm{d}s\right). \tag{2.16}$$

The PDF of the RDE solution (independent of parameter realizations) is finally obtained by marginalizing the joint PDF of both the solution and the random parameter vector $\mathbf{A}$, which, using the conditional PDF, can be written as

$$f(\mathbf{x}, t) = \int_{\mathbb{R}^m} f(\mathbf{x}, t\,|\,\mathbf{a})f_{\mathbf{A}}(\mathbf{a})\mathrm{d}\mathbf{a} = \mathbb{E}_{\mathbf{A}}[f(\mathbf{x}, t\,|\,\mathbf{A})], \tag{2.17}$$

where $f_{\mathbf{A}}$ is the joint PDF of the random vector parameters $\mathbf{A}$ and $\mathbb{E}_{\mathbf{A}}$ denotes the expectation operator with respect to $\mathbf{A}$. This shows that the PDF can be obtained by calculating (2.16) for all realizations $\mathbf{a}$ of $\mathbf{A}$ and then averaging. Furthermore, when computational techniques are required for this task, expression (2.17) allows the use of either quadrature formulas [49] or Monte Carlo simulations [50–53].

2.2.2 | PDF transformation at the impulse times

Let us turn back to the set of conditions in (2.11), which are identities between random variables. Now, we are going to make use of the RVT Theorem 1.1. As in the case of the pathwise solution analysis, let us consider the first transformation in detail, and then we will write the result for the general case.

Let $f(\cdot, t_1)$ be the PDF of the solution stochastic process at a given impulse time t_1 (which is unknown) and let $f(\cdot, t_1^-)$ be the PDF before the jump (which is known because it verifies the Liouville equation in the interval (t_0, t_1)). Using (2.7) we can compute the Jacobian of the variable transformation:

$$\mathbf{X}(t_1,\omega) + \boldsymbol{\Gamma}_1(\omega) = \mathbf{X}(t_1^-,\omega) \iff |J| = \left|\frac{\partial\mathbf{X}(t_1^-,\omega)}{\partial\mathbf{X}(t_1,\omega)}\right| = 1. \tag{2.18}$$

Denoting the joint PDFs of $\mathbf{X}(t,\cdot)$ and Γ_1 by $f_{(\mathbf{X}(t),\boldsymbol{\Gamma}_1)}$, for $t = t_1, t_1^-$, the application of the RVT theorem leads to

$$f_{(\mathbf{X}(t_1),\boldsymbol{\Gamma}_1)}(\mathbf{x},\boldsymbol{\gamma}_1,t_1) = f_{(\mathbf{X}(t_1^-),\boldsymbol{\Gamma}_1)}\left(\mathbf{x}+\boldsymbol{\gamma}_1,\boldsymbol{\gamma}_1,t_1^-\right)\cdot 1 = f\left(\mathbf{x}+\boldsymbol{\gamma}_1,t_1^-\right)f_{\boldsymbol{\Gamma}_1}(\boldsymbol{\gamma}_1),$$

because $\mathbf{X}(t_1^-,\cdot)$ is independent from $\boldsymbol{\Gamma}_1$, which only appears at the impulse time. Note that $\boldsymbol{\gamma}_1 = (\gamma_1^1, \ldots, \gamma_1^d)$. Finally, to obtain the PDF of $\mathbf{X}(t_1,\cdot)$, we marginalize respect to $\boldsymbol{\Gamma}_1$

$$f(\mathbf{x}, t_1) = \int_{\mathcal{D}(\boldsymbol{\Gamma}_1)} f\left(\mathbf{x}+\boldsymbol{\gamma}_1,t_1^-\right)f_{\boldsymbol{\Gamma}_1}(\boldsymbol{\gamma}_1)\mathrm{d}\boldsymbol{\gamma}_1 = \mathbb{E}_{\boldsymbol{\Gamma}_1}[f\left(\mathbf{x}+\boldsymbol{\Gamma}_1,t_1^-\right)], \tag{2.19}$$

for all $\mathbf{x}$, which shows that, at the jump, there is a translation of the PDF for every realization of $\boldsymbol{\Gamma}_1$. The average of these translations gives the PDF of $\mathbf{X}(t_1,\cdot)$. Note that, in (2.19), $\mathcal{D}(\boldsymbol{\Gamma}_1)$ denotes the domain of random vector $\boldsymbol{\Gamma}_1(\omega)$.

Now, the Liouville equation describes the evolution of the PDF (2.19) until the following impulse time t_2. Clearly, at any other impulse time, we will have the same case as for t_1:

$$f(\mathbf{x}, t_k) = \mathbb{E}_{\mathbf{\Gamma}_k}[f\left(\mathbf{x} + \mathbf{\Gamma}_k, t_k^-\right)],\ \forall \mathbf{x} \in \mathcal{D},\ k = 1, \dots, N, \tag{2.20}$$

because of the relations at (2.11).

3 | NUMERICAL TECHNIQUES

This section briefly overviews the numerical procedures used to compute the 1-PDF evolution and its statistical information. This section is especially important when computing the flow or inverse flow functions of the underlying RDE are not explicitly obtainable. Since the impulse-induced transformation of the PDF consists of a simple translation of the PDF in space, this section will deal with the numerical methods used between the impulse times.

3.1 | Lagrangian particle methods and interpolation

Lagrangian methods treat a PDE solution as a family of particles first initialized in a grid. Instead of working on a fixed grid, the evolution of the particles' initial position and the PDE solution value for every particle is simulated through time. The focus is centered on each particle's position and information rather than the information that a given position in space may give of the solution [54,55, Sec. 3.3.2]. These methods are widely used in science and engineering for the reasons explained in Remark 3.1.

Because of the Liouville equation's special nature, we can use these methods. Let us recall the characteristic equation system (2.13). This system can be easily solved by numerical integration methods such as the well-known Runge–Kutta scheme of fourth order (RK4, [56]). The system of ODEs to be solved is defined as

$$\begin{aligned} \frac{\mathrm{d}}{\mathrm{d}t}\phi_1(t) &= g_1(\Phi(t), t),\ \phi_1(0) = x_1^0, \\ &\vdots \\ \frac{\mathrm{d}}{\mathrm{d}t}\phi_d(t) &= g_n(\Phi(t), t),\ \phi_n(0) = x_d^0, \\ \frac{\mathrm{d}}{\mathrm{d}t}f(\Phi(t), t) &= -f(\Phi(t), t)\nabla_{\mathbf{x}} \cdot \mathbf{g}(\Phi(t), t),\ f(\Phi(0), 0) = f_0(\Phi_0), \end{aligned} \tag{3.1}$$

where $\mathbf{x}_0 = (x_1^0, \dots, x_d^0)$ is a point in $\mathbb{R}^d$, which represents the initial position of the particle to be simulated. Accordingly, the first d equations define the time evolution of the particle, whereas the last equation in (3.1) defines the evolution of the PDF value of the considered particle.

However, as explained in Cottet and Koumoutsakos [57] and Bosler et al. [58], particles must be re-interpolated into a grid every few time steps from the numerical integrator. The interpolation method used depends on the particular case under study. Thus, the particular interpolation method used in each example will be stated therein.

Remark 3.1. The Liouville equation is a PDE describing the advection of a quantity, in this case, probability. Although there are many ways to solve PDEs numerically, we have chosen this particle/characteristic equation approach because of several reasons:

(1) Particle methods do not add artificial numerical dissipation (see previous studies [47, 59, 60]).
(2) They are easily parallelizable.
(3) Contrarily to grid-based methods such as finite differences, finite volumes, and finite elements, particle methods do not have a grid-size-forced CFL time step limit. This allows performing simulations with a lower number of time steps, thus reducing the time needed for simulation and the computational burden. Instead, the time step limitation is determined by the accuracy of the numerical integrator used to obtain the characteristic curves and the interpolation scheme used to re-interpolate particles onto the underlying grid. For example, for RBF interpolation, the limitation is set by the property that the basis functions must overlap (see Bergdorf and Koumoutsakos [61] and Bergdorf [62]). For example, if the dynamics are very complex or separate particles rapidly, we will have to re-interpolate more frequently, thus limiting the time step used for the numerical integrator.

(4) The spatial dimension does not explicitly determine the computational complexity of the particle approach; instead, it is given by the number of particles and the re-interpolation step, which depends on the spatial dimension; however, there are very efficient ways of performing high-dimensional interpolation, such as radial basis function (RBF) interpolation (see Iske and Arnold [63]).

3.2 | Adaptive mesh refinement (AMR)

As was explained in the previous subsection, the forward evolution of the initial PDF is obtained by evolving individual particles that are first initialized in a grid. Therefore, obtaining a high-resolution PDF representation requires a fine grid initializing the particles. This implies that a vast amount of particles would have to be evolved and re-interpolated back onto the fine grid. Interestingly, the need for more particle initializations may not be the same throughout the whole domain; some areas may need more particles than others. Using a fine grid in the whole domain would result in an enormous computational burden. These kinds of problems are known as *multi-scale* problems.

This issue is not specific to the Liouville equation. In fact, this has been an area of intense research for some time now, specifically in the computational fluid dynamics field. AMR techniques are commonly used to overcome this difficulty. We have used a wavelet compression-based technique based on the same approach as in Bergdorf and Koumoutsakos [61].

3.3 | Confidence region computation

Confidence intervals provide a valuable tool for analyzing and predicting probabilistic methods. Although building confidence intervals in normally distributed random variables in a one-dimensional problem is a reasonably easy task, it is certainly not trivial when dealing with random variables under a nonstandard distribution or in higher dimensions. Mathematically, given a PDF $f : \mathbb{R}^d \to [0, +\infty)$, we define the following function:

$$K(\lambda) := \int_{\{f \geq \lambda\}} f(\mathbf{x}) \mathrm{d}\mathbf{x}, \ \ \lambda \in [0, \|f\|_\infty],$$

where $\{f \geq \lambda\} := \{\mathbf{x} \in \mathbb{R}^d \,|\, f(\mathbf{x}) \geq \lambda\}$ and $\|f\|_\infty = \sup\{f(\mathbf{x}) : \mathbf{x} \in \mathrm{supp}(f)\}$. The objective is to find a value, λ^*, such that $K(\lambda^*) = 1 - \alpha$, where $\alpha \in [0, 1]$ is the confidence level. If $\alpha = 0.05$, we will obtain a 95% confidence interval, whereas if $\alpha = 0$, we will obtain the so-called ensemble region. Assuming that $\{f = \lambda\}$ is a Lebesgue-null set for all $\lambda \in (0, \|f\|_\infty]$, (as it happens for every PDF f that is almost everywhere non-constant inside its support), it can be easily shown that the previous function is everywhere continuous in $[0, \|f\|_\infty]$ and non-increasing. To find the optimal value, we can apply, for example, the bisection method to the function $K(\lambda) - 1 + \alpha$ (see Burden et al. [64]). However, other higher order iterative methods might be used as well.

4 | EXAMPLES

In this section, we will illustrate the applicability and versatility of the theoretical findings developed in the previous sections. The first case will consider a linear scalar RDE whose flow and inverse flow functions can be explicitly computed. We will also consider the information that can be extracted from the computation of the evolution of the PDF.

The second case will deal with the Duffing oscillator model. This case will not have an explicit solution; therefore, we will have to use computational techniques to determine the PDF evolution and its relevant probabilistic information.

As it was assumed in the previous theoretical developments, we assume that $(\Omega, \mathcal{F}, \mathbb{P})$ denotes the complete probability space where all the random variables are defined.

Also, for approximating (2.17) and (2.20), we have used the normalized weighted mean, where the weights are given by the PDF of each parameter vector:

$$f(\mathbf{x}, t) \approx \frac{\sum_{i=1}^{N_\mathbf{A}} f(\mathbf{x}, t \,|\, \mathbf{a}_i) f_\mathbf{A}(\mathbf{a}_i)}{\sum_{i=1}^{N_\mathbf{A}} f_\mathbf{A}(\mathbf{a}_i)}, \ \ f(\mathbf{x}, t_k) \approx \frac{\sum_{i=1}^{N_{\mathbf{\Gamma}_k}} f(\mathbf{x} + \boldsymbol{\gamma}_i, t_k^-) f_{\mathbf{\Gamma}_k}(\boldsymbol{\gamma}_i)}{\sum_{i=1}^{N_{\mathbf{\Gamma}_k}} f_{\mathbf{\Gamma}_k}(\boldsymbol{\gamma}_i)}.$$

Here, $\{\mathbf{a}_i\}_{i=1}^{N_\mathbf{A}}$ is a partition of the domain of the random parameter vector $\mathbf{A}$ and, analogously, $\{\boldsymbol{\gamma}_i\}_{i=1}^{N_{\mathbf{\Gamma}_k}}$ is a partition of the domain of the random parameter vector $\mathbf{\Gamma}_k$. Notice that the above approximations are based on the fact that the sums in

the denominators approximate the integrals of PDFs, so whose value is 1, and the partitions to calculate the integral in the numerator and denominator can be taken with the same step, which has been canceled to provide simpler approximations.

Finally, regarding the computational execution technicalities, all computations have been done via a custom-built C-based CUDA library [65] on a desktop computer with an i9-10900K CPU (40 GB of RAM) and an 8 GB NVIDIA Quadro RTX 4000, which we will call *Computer 1*, and on a laptop computer with an AMD Ryzen 7 5800H (16 GB of RAM) and a 6 GB NVIDIA RTX 3060, which we will call *Computer 2*. Note that the greatest difference between both computers relies on the CPU, not the GPU. Both GPUs have similar performance, and simulations do not need a large amount of memory, so this is not a problem either.

4.1 | Scalar linear RDE

Linear ODEs are the simplest and among the most successful types of ODEs. This kind of ODEs verifies many properties, making them relatively easy to work with. Although most natural phenomena are modeled by nonlinear ODEs, there are some cases where one can consider the *linearization* of the ODE; that is, a linear ODE whose dynamic properties are the same as the original nonlinear ODE in a neighborhood of some time where the linearization is done. For example, when studying growth processes in biology or medicine, a linear model can be used to predict the growth at the initial stages, despite the fact that nonlinear behavior appears after some time and ends up governing the growth process asymptotically. A typical example is the logistic model, which is nonlinear but behaves like the Malthusian model, which is linear, at the initial times.

We consider the following impulsive random IVP:

$$\dot{X}(t,\omega) = A(\omega)X(t,\omega) + B(\omega) - \Gamma \sum_{i=1}^{N} \delta(t - T_i),\ t > 0, \tag{4.1}$$

$$X(0,\omega) = X_0(\omega), \tag{4.2}$$

where $\omega \in \Omega$ and X_0, B, and $A \neq 0$ a.s. are finite-variance random variables with preassigned PDFs denoted by f_0, f_B, and f_A, respectively. Also, $\Gamma \neq 0$ a.s. is a random variable with a known PDF f_Γ. For the sake of simplicity, we assume that X_0, A, B, and Γ are mutually independent.

Obtaining the pathwise flow is a relatively easy task. Let us fix $\omega \in \Omega$ and denote $x_0 = X_0(\omega)$, $a = A(\omega)$, $b = B(\omega)$, $\gamma = \Gamma(\omega)$. Using the well-known solution expression of linear ODEs, for $t \in [T_k, T_{k+1})$, we get

$$\phi(t; x_0, a, b) = \mathrm{e}^{at}\left(x_0 + \frac{b}{a} - \gamma \sum_{i=1}^{k} \mathrm{e}^{-aT_i}\mathrm{H}(t - T_i)\right) - \frac{b}{a},$$

which can be easily proven to be a solution of the random IVP (4.1)–(4.2) (classical between impulse times and weak globally). Analogously, solving the previous equation for x_0, the inverse flow has the following expression:

$$\psi(t; x, a, b) = \mathrm{e}^{-at}\left(x + \frac{b}{a} + \gamma \sum_{i=1}^{k} \mathrm{e}^{a(t-T_i)}\mathrm{H}(t - T_i)\right) - \frac{b}{a}. \tag{4.3}$$

The Liouville equation for this case is easily obtained

$$\partial_t f(x,t\,|\,a,b) + (ax + b)\partial_x f(x,t\,|\,a,b) = -a f(x,t\,|\,a,b),$$

and its solution, conditioned to every pair of realizations (a,b), is given by

$$f(x,t\,|\,a,b) = f_0(\psi(t;x,a,b))\mathrm{e}^{-at}, \tag{4.4}$$

where ψ is defined in (4.3).

To obtain the final 1-PDF, we have to compute the conditional expectation of (4.4) with respect to A and B as shown in expression (2.17):

$$f(x,t) = \mathbb{E}_{A,B}[f(x,t\,|\,A,B)] = \int_{D(B)}\int_{D(A)} f_0(\psi(t;x,a,b))\mathrm{e}^{-at} f_A(a) f_B(b)\mathrm{d}a\mathrm{d}b, \tag{4.5}$$

TABLE 1 Statistical information about the random model parameters in the linear impulsive random IVP (4.1)–(4.2).

Variable	Distribution	Mean	Std
X_0	Normal	0.17	0.015
A	Gamma	0.03	0.02
B	Uniform	0.04	0.02
Γ	Uniform	0.5	0.02

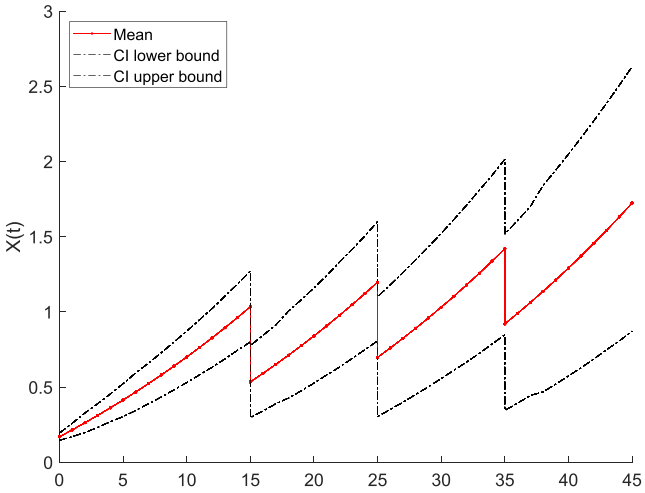

FIGURE 2 Mean function (red solid curve) of the solution process and the boundaries of the 95% confidence interval (black dashed curves). Linear impulsive random IVP (4.1)–(4.2) with random model parameters listed in Table 1. [Colour figure can be viewed at wileyonlinelibrary.com]

where $\mathcal{D}(A)$ and $\mathcal{D}(B)$ denote the domains of the random variables A and B, respectively.

Table 1 shows the chosen distributions, mean, and standard deviation (*Std* for short) of the parameter random variables. Note that these distributions have been selected just to illustrate the versatility of the Liouville equation method. Indeed, any other combination of probability distributions could have been chosen for the same purpose. We have considered 3 impulse times, at instants $T_1 = 15$, $T_2 = 25$, and $T_3 = 35$, with the same impulse strength distribution Γ.

Figure 2 shows the evolution of the mean function and the 95% confidence interval. We can see the characteristic exponential growth of the linear ODE (4.1) and the sharp decreases of the solution at the impulse times. We can also observe that the confidence interval size remains almost the same before and after the impulse, as expected from (2.20). This implies that there is almost no difference in the uncertainty of the system before and after a given impulse. Figure 3 shows the PDF at several time instants together with the information from Figure 2. This figure clearly shows the effect of the exponential growth determined by the linear ODE; indeed, as time goes on, each "slice" of the PDF becomes lower and wider (platykurtic) until it becomes a small lump when compared with the initial PDF where is leptokurtic. At $t = 15$, there is a sharp translation of the PDF, which is the effect of a Dirac impulse term. This fact can be further seen in Figure 4, which shows the transformations of the PDFs at each impulse time. Notice there is a translation of the PDF and a slight rescaling of the PDF, as expected by relation (2.20).

The elapsed time of the computation was ∼3.35 s on *Computer 1* and ∼4 s on *Computer 2*. For the simulation shown in Figures 2 and 3, we have used a 0.25 time step, with re-interpolation every four time steps. The grid is formed by 1024 equispaced nodes. It was computed using 150 samples (15 for parameter A and 10 for parameter B). Jumps were resolved using 30 samples for Γ (other combinations of samples can also be used).

4.2 | Random Duffing oscillator

Nonlinear oscillators have been thoroughly studied due to their rich dynamical behavior and ability to model a wide variety of natural and engineering phenomena. For example, Hooke's law states that there is a linear relationship between the deformation and the force exerted by a spring. However, when the deformation becomes large enough, the response becomes nonlinear. Also, elastic pendulums, mechanical isolators, beams with nonlinear stiffness, cable vibrations, and some electrical circuits can be modeled via the nonlinear oscillator equation known as the Duffing equation [66–68].

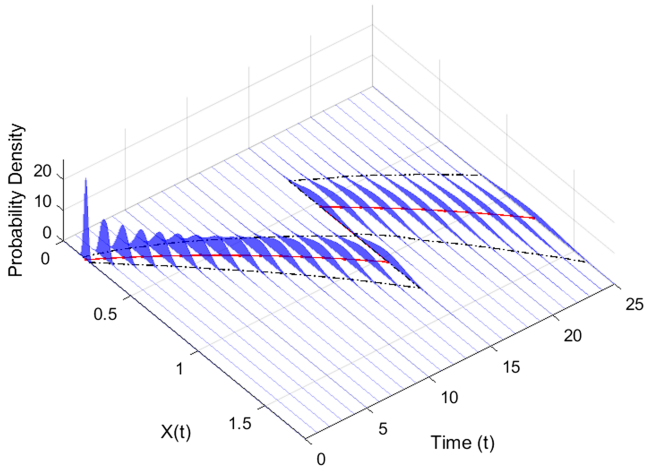

FIGURE 3 Waterfall plot of the evolution of the PDF (blue slices) with the mean function (red solid curve) and the confidence intervals (black dashed curves) in the time interval [0, 24]. Linear impulsive random IVP (4.1)–(4.2) with random model parameters listed in Table 1. [Colour figure can be viewed at wileyonlinelibrary.com]

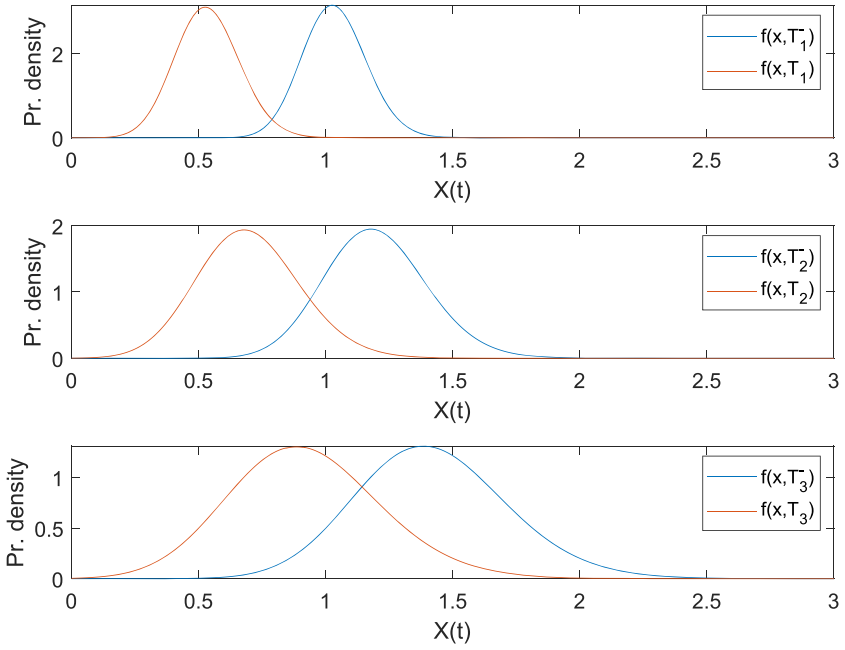

FIGURE 4 PDFs before and after each of the three impulse times: $T_1 = 15$, $T_2 = 25$, and $T_3 = 35$. Linear impulsive random IVP (4.1)–(4.2) with random model parameters listed in Table 1. [Colour figure can be viewed at wileyonlinelibrary.com]

We here consider the following impulse-forced Duffing equation:

$$\ddot{X}(t,\omega) + 2\Xi(\omega)\dot{X}(t) + X(t,\omega) + \Lambda(\omega)X(t,\omega)^3 = \sum_{i=1}^{N} \Gamma_i(\omega)\delta(t - T_i),\ t > 0, \tag{4.6}$$

$$X(0,\omega) = X_0(\omega),\ \dot{X}(0,\omega) = \dot{X}_0(\omega), \tag{4.7}$$

where the model parameters $\Xi > 0$ and $\Lambda > 0$, as well as the initial conditions X_0 and $\dot{X}_0$, are assumed to be mutually independent finite-variance random variables with preassigned PDFs f_Ξ, f_Λ, f_{X_0}, and $f_{\dot{X}_0}$, respectively. Also, the random variables $\{\Gamma_i\}_{i=1}^N$ are assumed to be mutually independent with known PDFs denoted by f_{Γ_i}, $i = 1, \ldots, N$.

Contrarily to the previous example, the Duffing model does not have an "easily manageable" closed-form solution, and furthermore, the cases where such a solution expression exists are rare [69]. Therefore, this case will be treated

numerically. In this context, combining the RVT method and the Liouville equation is particularly useful rather than only applying the RVT method.

First, let us transform the Duffing equation into a first-order two-dimensional ODE. Consider the vector $\mathbf{Y}(t,\omega) = [Y_1, Y_2]^\mathsf{T} := [X(t,\omega), \dot{X}(t,\omega)]^\mathsf{T}$, $t \geq 0$, whose components represent position and velocity, respectively. Now, dropping the ω-notation, the Duffing equation can be written as

$$\dot{\mathbf{Y}}(t) = \begin{bmatrix} Y_2(t) \\ -2\Xi Y_2(t) - Y_1(t) - \Lambda Y_1(t)^3 + \sum_{i=1}^{N} \Gamma_i \delta(t - T_i) \end{bmatrix}, \quad \mathbf{Y}(0) = \begin{bmatrix} X_0 \\ \dot{X}_0 \end{bmatrix},$$

where $\dot{\mathbf{Y}}$ can be rewritten as

$$\dot{\mathbf{Y}}(t) = \overbrace{\begin{bmatrix} Y_2(t) \\ -2\Xi Y_2(t) - Y_1(t) - \Lambda Y_1(t)^3 \end{bmatrix}}^{\mathbf{g}(\mathbf{Y}(t),t,\Xi,\Lambda)} + \sum_{i=1}^{N} \delta(t - T_i) \overbrace{\begin{bmatrix} 0 \\ \Gamma_i \end{bmatrix}}^{\boldsymbol{\Gamma}_i}.$$

TABLE 2 Statistical information about the random model parameters in the Duffing equation.

Variable	Mean	Std.
X_0	1.75	0.025
$\dot{X}_0$	0	0.025
Ξ	0.2	0.02
Λ	3	0.3
Γ_1	2.5	0.02
Γ_2	1	0.02
Γ_3	1.2	0.02

Note: In all the cases, random variables are assumed to be independent and have Normal distributions with the specified values for the mean and the variance. Due to their physical meaning, the random variables Ξ and Λ are truncated to positive values. Random Duffing oscillator (4.6)–(4.7).

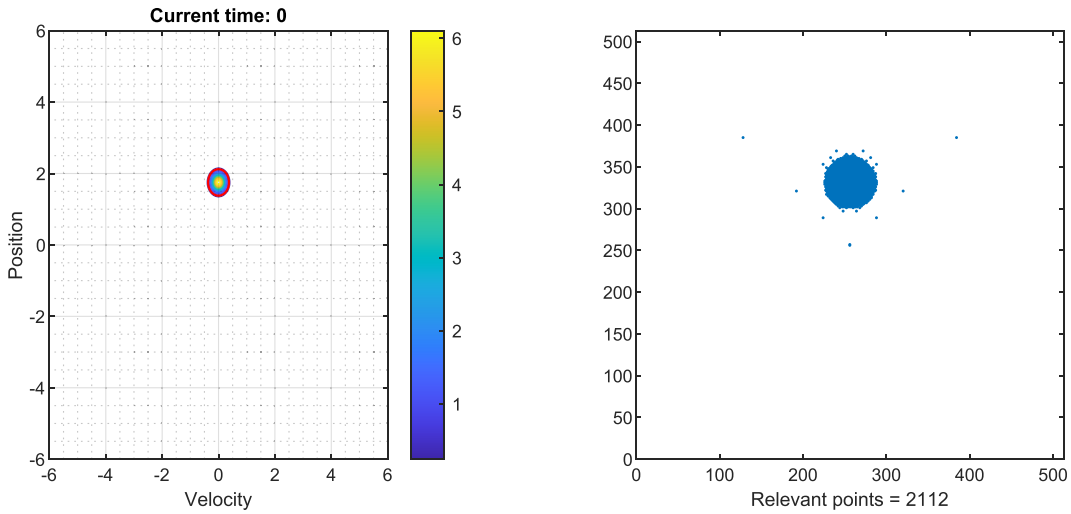

FIGURE 5 Left: Level curves of the initial PDF f_0 (view color bar) of the Duffing equation model and the 95% confidence region (curve in red). Right: Scatter view of the grid points that will be used to compute the evolution of the PDF. We obtain a 99.43% compression with respect to the underlying fine grid. Random Duffing oscillator (4.6)–(4.7) with random model parameters listed in Table 2. [Colour figure can be viewed at wileyonlinelibrary.com]

As we will simulate the initial PDF evolution numerically, we have to build the Liouville equation to be solved between the impulse times and then translate the PDF as shown in (2.20). Let us fix $\omega \in \Omega$ and consider the pair of arbitrary realizations $\xi = \Xi(\omega)$ and $\lambda = \Lambda(\omega)$. Indeed, the vector field and divergence terms for the Liouville equation are

$$\mathbf{g}(y_1, y_2, t, \xi, \lambda) = (y_2, -2\xi y_2 - y_1 - \lambda y_1^3), \ \nabla_{\mathbf{y}} \cdot \mathbf{g}(y_1, y_2, t, \xi, \lambda) = -2\xi,$$

respectively. Therefore, the Liouville equation related to the random IVP (4.1)–(4.2) between the impulse times is

$$\partial_t f(\mathbf{y}, t \,|\, \xi, \lambda) + y_2 \partial_{y_1} f(\mathbf{y}, t \,|\, \xi, \lambda) - (2\xi y_2 + y_1 + \lambda y_1^3) \partial_{y_2} f(\mathbf{y}, t \,|\, \xi, \lambda) = 2\xi f(\mathbf{y}, t \,|\, \xi, \lambda), \tag{4.8}$$

$$f(\mathbf{y}, 0 \,|\, \xi, \lambda) = f_0(\mathbf{y}) := f_{X_0}(y_1) f_{\dot{X}_0}(y_2). \tag{4.9}$$

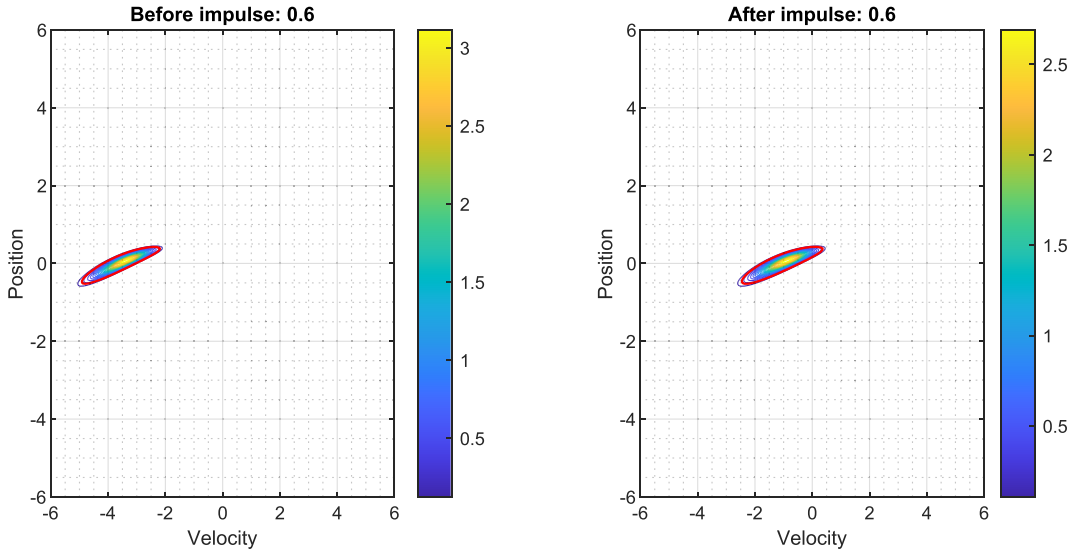

FIGURE 6 Left: PDF approaching the first impulse time from the left, that is, $f(\cdot, 0.6^-)$. Right: PDF at the transformation, that is, $f(\cdot, 0.6) = f(\cdot, 0.6^+)$. Random Duffing oscillator (4.6)–(4.7) with random model parameters listed in Table 2. [Colour figure can be viewed at wileyonlinelibrary.com]

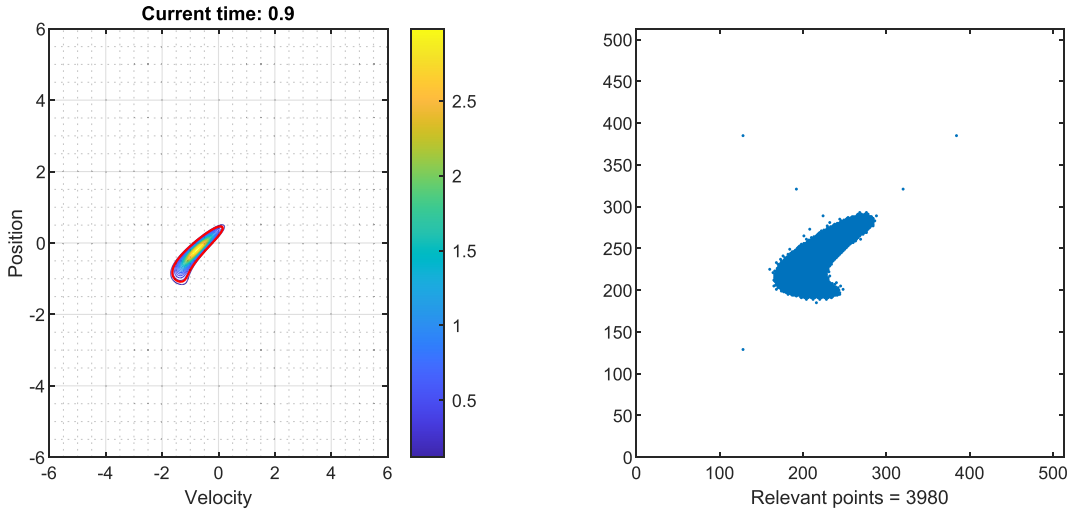

FIGURE 7 Left: Level curves of the PDF at time $t = 0.9$ (view color bar) and the 95% confidence region (curve in red). Right: Scatter view of the relevant grid points for the computation of the evolution of the PDF. We obtain a 98.79% compression with respect to the underlying fine grid. Random Duffing oscillator (4.6)–(4.7) with random model parameters listed in Table 2. [Colour figure can be viewed at wileyonlinelibrary.com]

In order to solve this PDE, we will make use of the Lagrangian particle and AMR techniques described in Sections 3.1 and 3.2, respectively. Finally, as mentioned at the end of Section 2.2.1, all that would be left is to compute the PDF marginalizing the model parameters Ξ and Λ using expression (2.17) with the identification $\mathbf{A} = (\Xi, \Lambda)$.

To carry out the computations, we have assumed the probability distributions listed in Table 2 for each random variable. Note that we have considered three impulse terms, which have been chosen at the following time values: $T_1 = 0.6$, $T_2 = 1.2$, and $T_3 = 2.4$. Furthermore, in Figures 5–11, we show the evolution of the initial PDF for the corresponding parameter distributions before and at the corresponding impulse times.

These simulations show the fascinating dynamics induced by the Duffing oscillator. The complete sequence of Figures 5–11 (left figures) show the initial joint PDF for the position and velocity (that is shown in Figure 5 [left]) begins to decay in a counter-clockwise spiral-like fashion toward the origin, which is its trivial equilibrium point. As it is shown in the right figure in Figures 5,7,9, and 11, the AMR technique selects relatively few points as the particles that will be

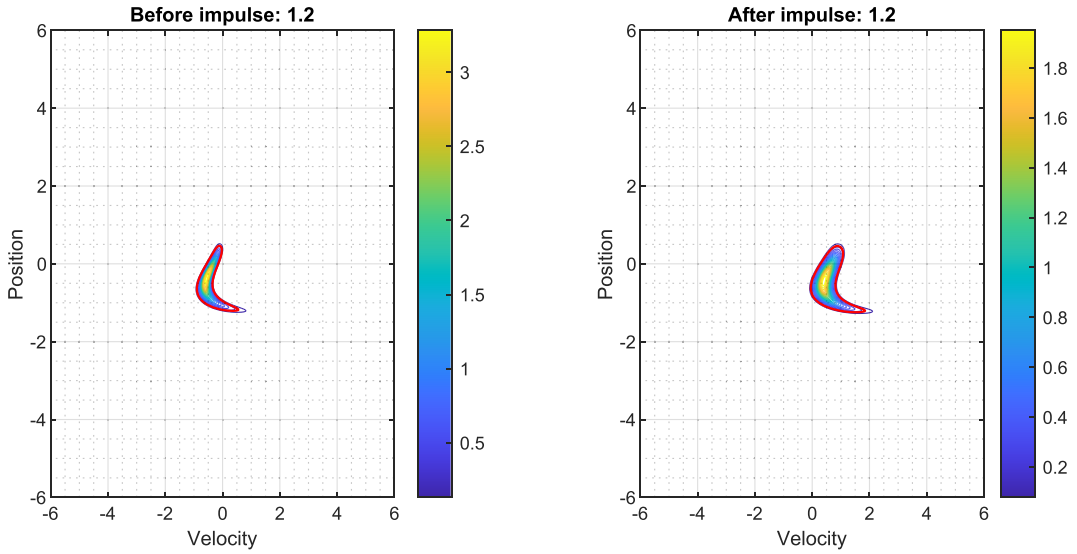

FIGURE 8 Left: PDF approaching the second impulse time from the left, that is, $f(\cdot, 1.2^-)$. Right: PDF at the transformation, that is, $f(\cdot, 1.2) = f(\cdot, 1.2^+)$. Random Duffing oscillator (4.6)–(4.7) with random model parameters listed in Table 2. [Colour figure can be viewed at wileyonlinelibrary.com]

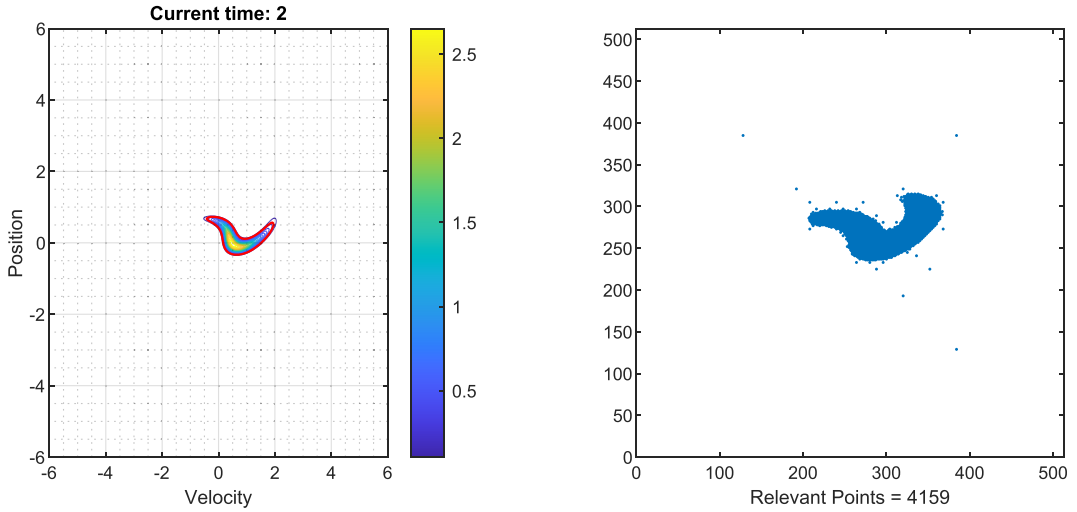

FIGURE 9 Left: Level curves of the PDF at time $t = 2$ (view color bar) and the 95% confidence region (curve in red). Right: Scatter view of the relevant grid points for the computation of the evolution of the PDF. We obtain a 98.72% compression with respect to the underlying fine grid. Random Duffing oscillator (4.6)–(4.7) with random model parameters listed in Table 2. [Colour figure can be viewed at wileyonlinelibrary.com]

evolved using the corresponding characteristic equations (3.1). These points carry the most information about the values of the PDF in the underlying 512×512-point grid.

Figure 6 shows the joint PDF of position and velocity before the first impulse time $T_1 = 0.6$ (left figure) and its transformation after applying the impulse (left figure). We can see that the transformation (all of them) consists of a translation and a subtle rescaling due to the distribution of the impulse random variable Γ_1. If the impulse were deterministic, the transformation would consist of a translation only (compare with 2.20).

As explained in Section 2.2, the simulation continues by performing the AMR of the transformed PDF and smoothly evolving the PDF until the next impulse time. As it can be seen in Figure 7, the PDF starts to lose its ellipse-like shape because the points that are further away from the origin carry more velocity than those where the PDF is concentrated. This fact is clearly observable when we arrive at the next impulse time, $T = 1.2$ (Figure 8). Now, the aforementioned

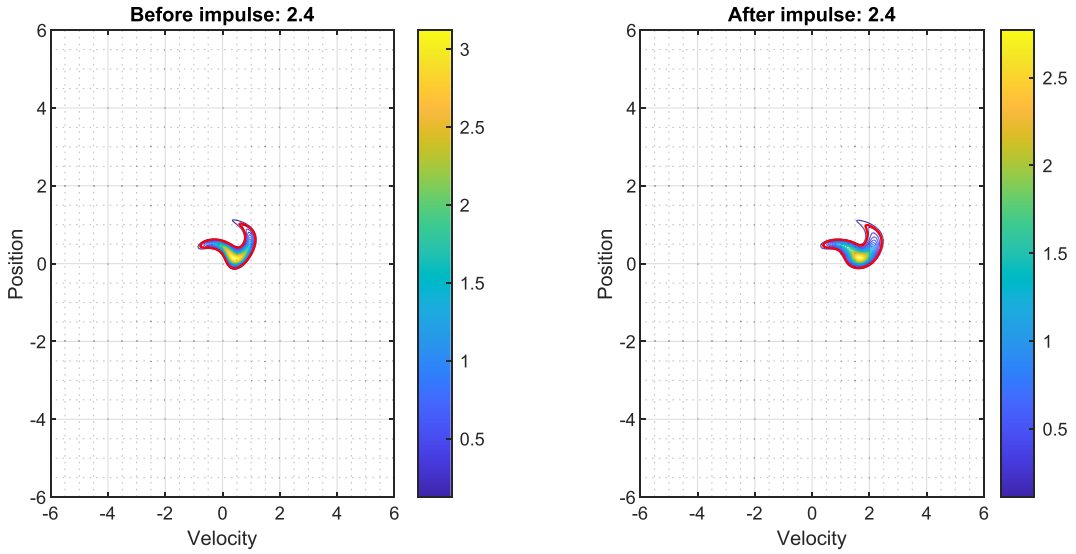

FIGURE 10 Left: PDF approaching the third impulse time from the left, that is, $f(\cdot, 2.4^-)$. Right: PDF at the transformation, that is, $f(\cdot, 2.4) = f(\cdot, 2.4^+)$. Random Duffing oscillator (4.6)–(4.7) with random model parameters listed in Table 2. [Colour figure can be viewed at wileyonlinelibrary.com]

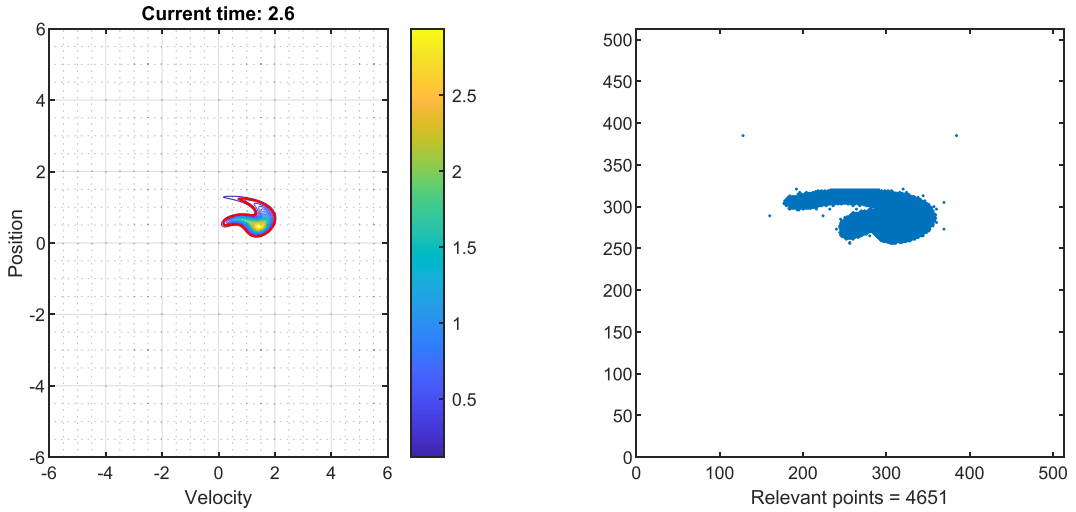

FIGURE 11 Left: Level curves of the PDF at time 2.6 (view color bar) and the 95% confidence region (curve in red). Right: Scatter view of the relevant grid points for the computation of the evolution of the PDF. We obtain a 98.48% compression with respect to the underlying fine grid. Random Duffing oscillator (4.6)–(4.7) with random model parameters listed in Table 2. [Colour figure can be viewed at wileyonlinelibrary.com]

rescaling property is visible on the plot. There is a greater difference between the PDF before and after the impulse time than in the first impulse (compare Figures 6 and 8).

Once again, the AMR is performed, and the PDF evolves from its new state according to the Duffing oscillator dynamics. Figure 9 shows the interesting form that the PDF is attaining. Finally, the last impulse transformation at time $T = 2.4$ is shown in Figure 10, and Figure 11 shows the peculiar form of the PDF at time $t = 2.6$. Figure 12 shows the marginal PDF of position at time $t = 2.6$, assuming a fixed value for velocity 0.6 (compare with Figure 11) whereas Figure 13 shows the marginal PDF of velocity at time $t = 2$, assuming that position is in the interval $[0.4, 0.6]$. As mentioned in the introduction, by knowing the joint PDF of a stochastic process, we can understand its behavior at every time instant. These figures shown in this example are a clear example where knowing the joint and marginal PDFs gives statistical information that would not be attainable by computing only the mean and variance of the stochastic process, as is usually done in the literature.

As a final note regarding the interpolation procedure used in this particular case, we have used compactly supported RBF interpolation based on the Wendland C^2 kernels [63]. Although there may be faster methods for interpolating scattered points in 2D, RBF-based interpolation allows for a stable, easily implementable, and general interpolation approach, independently of the dimensionality of the RDE system. Also, the time step used for the numerical solution via the Runge–Kutta integrator is 0.05, and we have re-interpolated the particles every two steps. We have seen (heuristically)

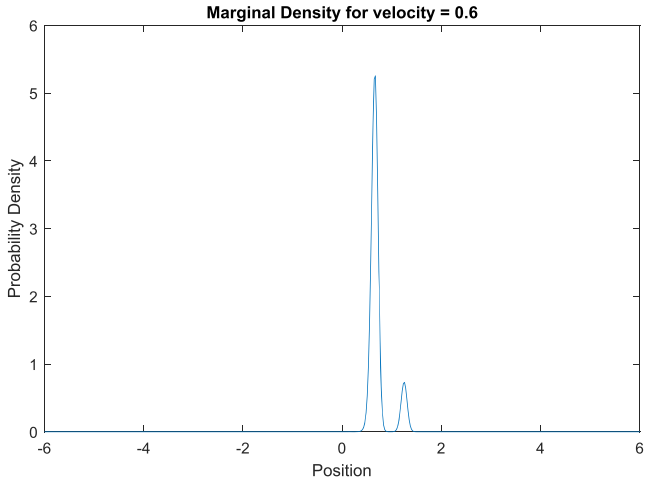

FIGURE 12 Marginal PDF of position at time $t = 2.6$, that is, $X(2.6)$, subject to $\dot{X}(2.6) = 0.6$. Random Duffing oscillator (4.6)–(4.7) with random model parameters listed in Table 2. [Colour figure can be viewed at wileyonlinelibrary.com]

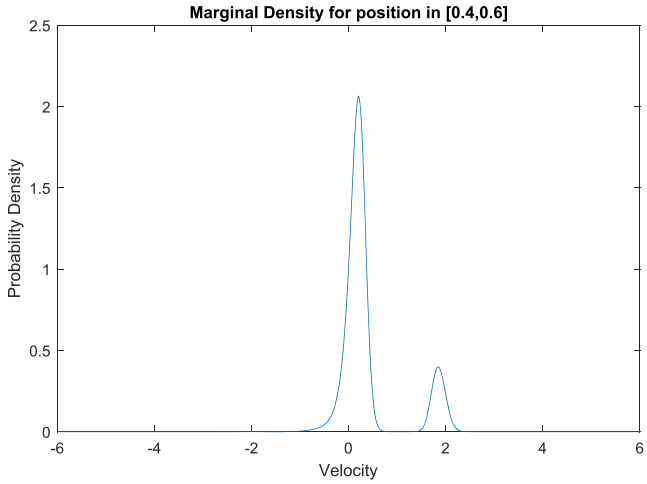

FIGURE 13 Marginal PDF of velocity at time $t = 2$, that is, $\dot{X}(2)$, subject to $X(2.6) \in [0.4, 0.6]$. Random Duffing oscillator (4.6)–(4.7) with random model parameters listed in Table 2. [Colour figure can be viewed at wileyonlinelibrary.com]

that these values give an acceptable trade-off between accuracy and computational efficiency. The timing of the simulation was ∼48.3 s on *Computer 1* and ∼71.6 s on *Computer 2*. In this case, we used 98 samples (7 for Ξ and 14 for Λ, although other combinations can be used). Jumps were resolved using 20 samples each.

5 | CONCLUSIONS AND FUTURE WORK

In this contribution, we have studied the evolution of probability density functions determined by a stochastic process verifying a general class of RDE systems with Dirac delta-like impulses. We have done so by studying the behavior of the sample trajectories of the system via the Laplace transform. Afterward, using the Liouville equation and the RVT theorem, we have been able to use the sample-trajectory information to understand how the probability density function evolves between impulse times and at the impulse times, respectively. Finally, to show the applicability and generality of this method, we have applied the theoretical findings to two commonly used models in applied mathematics, considering random parameters and impulse strengths.

The main conclusion of our study is that the combination of Liouville's PDE and the RVT method is a promising strategy to perform a complete UQ of nonlinear RDEs via the approximation of its 1-PDF. The method may open new avenues for approximating higher order probability density functions associated with the solution of RDEs. In particular, it would allow the approximation of multidimensional moments of the solution. For example, by extending the strategy developed in this paper to higher dimensions to approximate the second probability density function, one would obtain the correlation function of the solution, which accounts for valuable information about the corresponding random system.

On the one hand, regarding the limitations of our work, we are aware that using compactly supported RBFs as interpolation kernels could be a limiting factor when simulating the evolution of piecewise constant densities, such as uniform distributions. Another issue we are currently working on is that Lagrangian particle simulations are not volume conserving. Therefore, when re-interpolating onto the underlying grid, some probability is lost. On the other hand, regarding future work, our primary goal is to apply this approach to real-world problems using real data. In that sense, we will study how to link this "Liouville solver" to state-of-the-art optimization techniques such as multi-objective particle swarm optimization, which we have been working on lately.

ACKNOWLEDGEMENTS

This work has been partially supported by the Spanish Ministerio de Economía, Industria y Competitividad (MINECO), the Agencia Estatal de Investigación (AEI), Fondo Europeo de Desarrollo Regional (FEDER UE) (Grant PID2020-115270GB-I00), the Generalitat Valenciana (Grant AICO/2021/302), el Fondo Social Europeo y la Iniciativa de Empleo Juvenil (EDGJID/2021/185), Ayuda a Primeros Proyectos de Investigación (PAID-06-22), and Vicerrectorado de Investigación de la Universitat Politécnica de Valéncia (UPV). Vicente Bevia acknowledges the doctorate scholarship granted by Programa de Ayudas de Investigación y Desarrollo (PAID), Universitat Politécnica de Valéncia (UPV).

CONFLICT OF INTEREST STATEMENT

This work does not have any conflicts of interest.

ORCID

Vicente J. Bevia https://orcid.org/0000-0002-6034-6324
Juan C. Cortés https://orcid.org/0000-0002-6528-2155
Rafael J. Villanueva https://orcid.org/0000-0002-0131-0532

REFERENCES

1. A. D. Kiureghian and O. Ditlevsen, *Aleatory or epistemic? Does it matter?* Struct. Safety **31** (2009), 105–112.
2. R. C. Smith, *Uncertainty quantification: theory, implementation and applications*, Computational Science and Engineering, SIAM, New York, 2014.
3. D. Xiu, *Numerical methods for stochastic computations: a spectral method approach*, Computational Science and Engineering, Princeton University Press, New Jersey, 2010.
4. T. T. Soong, *Random differential equations in science and engineering*, Academic Press, New York, 1973.

5. H. Evans and P. E. Kloeden, *Random ordinary differential equations and their numerical solution*, Probability Theory and Stochastic Modelling, Springer Singapore, Singapore, 2017.
6. T. Neckel and F. Rupp, *Random differential equations in scientific computing*, De Gruyter Open, München, 2013.
7. M.-C. Casabán, J.-C. Cortés, J.-V. Romero, and M.-D. Roselló, *Solving random homogeneous linear second-order differential equations: a full probabilistic description*, Mediterranean J. Math. **13** (2016), 3817–3836.
8. F. A. Dorini, M. S. Cecconello, and L. B. Dorini, *On the logistic equation subject to uncertainties in the environmental carrying capacity and initial population density*, Commun. Nonlin. Sci. Numer. Simul. **33** (2016), 160–173.
9. J. Calatayud, J.-C. Cortés, and M. Jornet, *Uncertainty quantification for random parabolic equations with nonhomogeneous boundary conditions on a bounded domain via the approximation of the probability density function*, Math. Methods Appl. Sci. **42** (2019), 5649–5667.
10. F. A. Dorini and M. C. C. Cunha, *On the linear advection equation subject to random velocity fields*, Math. Comput. Simul. **82** (2011), 679–690.
11. A. Hussein and M. M. Selim, *Solution of the stochastic generalized shallow-water wave equation using RVT technique*, Eur. Phys. J. Plus **130** (2015), 249.
12. H. Slama, A. Hussein, N. A. El-Bedwhey, and M. M. Selim, *An approximate probabilistic solution of a random SIR-type epidemiological model using RVT technique*, Appl. Math. Comput. **365** (2019), 144–156.
13. A. Hussein, H. Slama, and M. M. Selim, *A full probabilistic solution of a stochastic red blood cells model using RVT technique*, European Phys. J. Plus **136** (2021), 381.
14. T. Caraballo, J.-C. Cortés, and A. Navarro-Quiles, *Applying the random variable transformation method to solve a class of random linear differential equation with discrete delay*, Appl. Math. Comput. **356** (2019), 198–218.
15. C. Burgos, J.-C. Cortés, L. Villafuerte, and R.-J. Villanueva, *A mean square convergent numerical solutions of random fractional differential equations: approximations of moments and density*, J. Comput. Appl. Math. **378** (2020), 112925.
16. T. Caraballo, M. Hammami, and L. Mchiri, *Practical exponential stability of impulsive stochastic functional differential equations*, Syst. Control Lett. **109** (2017), 43–48.
17. L. Hu, Y. Ren, and R. Sakthivel, *Stability of square-mean almost automorphic mild solutions to impulsive stochastic differential equations driven by G-Brownian motion*, Int. J. Control **93** (2020), 3016–3025.
18. S. Liu, A. Debbouche, and J. Wang, *On the iterative learning control for stochastic impulsive differential equations with randomly varying trial lengths*, J. Comput. Appl. Math. **312** (2017), 47–57.
19. J.-C. Cortés, S. E. Delgadillo-Alemán, R. Kú-Carrillo, and R.-J. Villanueva, *Probabilistic analysis of a class of impulsive linear random differential equations via density functions*, Appl. Math. Lett. **121** (2021), 107519.
20. J.-C. Cortés, S. E. Delgadillo-Alemán, R. Kú-Carrillo, and R.-J. Villanueva, *Full probabilistic analysis of random first-order linear differential equations with Dirac delta impulses appearing in control*, Math. Methods Appl. Sci. (2021), 1-20. DOI 10.1002/mma.7715
21. J. Calatayud, J. Carlos Cortés, and M. Jornet, *Computing the density function of complex models with randomness by using polynomial expansions and the RVT technique. Application to the SIR epidemic model*, Chaos Solitons Fractals **133** (2020), 109639.
22. V. Bevia, J. C. Cortés, M. Jornet, and R. J. Villanueva, *Probabilistic analysis of a general class of nonlinear random differential equations with state-dependent impulsive terms via probability density functions*, Commun. Nonlin. Sci. Numer. Simul. **119** (2023), 107097. https://www.sciencedirect.com/science/article/pii/S1007570423000151
23. V. Bevia, C. Burgos, J. C. Cortés, A. Navarro-Quiles, and R.-J. Villanueva, *Uncertainty quantification analysis of the biological Gompertz model subject to random fluctuations in all its parameters*, Chaos, Solitons Fractals **138** (2020), 109908.
24. V. Bevia, C. Burgos, J. C. Cortés, A. Navarro, and R. J. Villanueva, Analysing differential equations with uncertainties via the Liouville-Gibbs theorem: theory and applications, *Computational mathematics and applications*, D. Zeidan, S. Padhi, A. Burqan, and P. Ueberholz, (eds.), Springer Singapore, Singapore, 2020, pp. 1–23. DOI 10.1007/978-981-15-8498-5_1
25. F. Santambrogio, *Optimal transport for applied mathematicians. calculus of variations, PDEs and modeling*, Birkhäuser, Cham, 2015.
26. B. W. Silverman, *Density estimation for statistics and data analysis*, Chapman & Hall, London, 1986.
27. J. C. Cortés and M. Jornet, *Improving kernel methods for density estimation in random differential equations problems*, Math. Comput. Appl. **25** (2020), 109639.
28. S. Hu, *Propagation of uncertainty in dynamical systems*, Proceedings of the 43rd ISCIE International Symposium on Stochastic Systems Theory and its Applications, The ISCIE Symposium on Stochastic Systems Theory and Its Applications, Shiga, Japan, 2012, pp. 134–139.
29. F. Kozin, *On the probability densities of the output of some random systems*, J. Appl. Mech. **28** (1961), 161–165.
30. T. Saaty, *Modern nonlinear equations*, Dover Publications, New York, 1973.
31. J. B. Chen and J. Li, *A note on the principle of preservation of probability and probability density evolution equation*, Probabilist. Eng. Mech. **24** (2009), 51–59.
32. M. Jornet, *Liouville's equations for random systems*, Stochast. Anal. Appl. **40** (2022), 1026–1047.
33. M. Souaiby, A. Tanwani, and D. Henrion, *Ensemble approximations for constrained dynamical systems using Liouville equation*, Automatica **149** (2023), 110836. https://www.sciencedirect.com/science/article/pii/S0005109822007038
34. M. Ehrendorfer, *The Liouville equation and its potential usefulness for the prediction of forecast skill. Part I: theory*, Mon. Weather Rev. **122** (1994), 703–713.
35. M. Ehrendorfer, *The Liouville equation and its potential usefulness for the prediction of forecast skill. Part II: applications*, Mon. Weather Rev. **122** (1994), 714–728.

36. M. Ehrendorfer, The Liouville equation and atmospheric predictability, *Predictability of weather and climate*, Cambridge University Press, Cambridge, UK, 2006, pp. 59–98.
37. R. Weisman, M. Majji, and K. T. Alfriend, *Solution of Liouville's equation for uncertainty characterization of the main problem in satellite*, CMES-Comput. Modeling Eng. Sci. **111** (2016), 269–304.
38. V. Tarasov, *Liouville and Bogoliubov equations with fractional derivatives*, Modern Phys. Lett. B **21** (2007), 237–248.
39. M. Loève, *Probability theory I*, Springer, New York, NY, 1977.
40. C. Gasquet and P. Witomski, *Fourier analysis and applications. Filtering, numerical computation, wavelets*, Springer, New York, 1998.
41. J. Peano, *Démonstration de l'intégrabilité des équations différentielles ordinaires*, Mathematische Annalen **37** (1890), 182–228.
42. G. Teschl, *Ordinary differential equations and dynamical systems*, American Mathematical Society, Providence, R.I., 2012.
43. R. P. Agarwal and V. Lakshmikantham, *Uniqueness and nonuniqueness criteria for ordinary differential equations*, Series in Real Analysis, World Scientific, Singapore, 1993. https://books.google.es/books?id=q4OkW4H8BCUC
44. P. Dyke, *An introduction to laplace transforms and fourier series*, Springer, London, 2014.
45. J. J. Benedetto, *Harmonic analysis and applications*, CRC Press, Boca Raton, 1997.
46. L. C. Evans, *Partial differential equations*, American Mathematical Society, Providence, RI, 2010.
47. V. J. Bevia, C. Burgos, J. C. Cortés, and R. J. Villanueva, *Uncertainty quantification of random microbial growth in a competitive environment via probability density functions*, Fractal Fract. **5** (2021), no. 2, 26.
48. L. Hörmander, *The analysis of linear partial differential operators I: distribution theory and fourier analysis*, Springer, Berlin, Heidelberg, 2003.
49. P. J. Davis and P. Rabinowitz, *Methods of numerical integration*, Dover Books, San Diego, 2007.
50. D. P. Kroese, T. J. Brereton, T. Taimre, and Z. I. Botev, *Why the Monte Carlo method is so important today*, Wiley Interdisciplin. Rev.: Comput. Stat. **6** (2014), no. 6, 386–392.
51. R. E. Caflisch, *Monte Carlo and quasi-Monte Carlo methods*, Acta Numer. **7** (1998), 1–49.
52. W. J. Morokoff and R. E. Caflisch, *Quasi-Monte Carlo integration*, J. Comput. Phys. **122** (1995), no. 2, 218–230. https://www.sciencedirect.com/science/article/pii/S0021999185712090
53. M. B. Giles, *Multilevel Monte Carlo methods*, Acta Numer. **24** (2015), 259–328.
54. G. K. Batchelor, *An introduction to fluid dynamics*, Cambridge University Press, Cambridge, UK, 1973.
55. T. T. Warner, *Numerical weather and climate prediction*, Cambridge University Press, Cambridge, UK, 2012.
56. J. C. Butcher, *Runge–Kutta methods*, John Wiley & Sons, Ltd, West Sussex, 2016.
57. G. H. Cottet and P. Koumoutsakos, *High order semi-Lagrangian particle methods*, Spectral and High Order Methods for Partial Differential Equations ICOSAHOM 2016 *Edited by* M. L. Bittencourt, N. A. Dumont, and J. S. Hesthaven, Springer International Publishing, Cham, 2017, pp. 103–117.
58. P. A. Bosler, J. Kent, R. Krasny, and C. Jablonowski, *A Lagrangian particle method with remeshing for tracer transport on the sphere*, J. Comput. Phys. **340** (2017), 639–654. https://www.sciencedirect.com/science/article/pii/S002199911730253X
59. S. Koshizuka, K. Shibata, M. Kondo, and T. Matsunaga, Chapter 1—Introduction, *Moving particle semi-implicit method*, S. Koshizuka, K. Shibata, M. Kondo, and T. Matsunaga, (eds.), Academic Press, London, 2018, pp. 1–23. https://www.sciencedirect.com/science/article/pii/B9780128127797000011
60. P. Schreurs, J. Mewis, and J. Havens, *Numerical aspects of a lagrangian particle model for atmospheric dispersion of heavy gases*, J. Hazardous Mater. **17** (1987), no. 1, 61–80. https://www.sciencedirect.com/science/article/pii/0304389487850422
61. M. Bergdorf and P. Koumoutsakos, *A Lagrangian particle-wavelet method*, Multiscale Modeling Simul. **5** (2006), no. 3, 980–995.
62. M. E. Bergdorf. (2007). *Multiresolution particle methods for the simulation of growth and flow*, Doctoral Thesis, ETH Zürich, Zürich.
63. A. Iske and V. I. Arnold, *Multiresolution methods in scattered data modelling*, Springer-Verlag, Berlin, 2004.
64. A. Burden, R. Burden, and J. Faires, *Numerical analysis*, 10th ed., Cengage Learning, Boston, 2016.
65. V. J. Bevia, *N-dimensional Liouville Solver [Computer Software]*, 2023. DOI 10.5281/zenodo.7673678 [Accessed: February 2023].
66. I. Kovacic and M. Brennan, *The Duffing equation: nonlinear oscillators and their behavior*, John Wiley & Sons, West Sussex, 2011.
67. Y. Jia, *Review of nonlinear vibration energy harvesting: Duffing, bistability, parametric, stochastic and others*, J. Intell. Material Syst. Struct. **31** (2020), no. 7, 921–944.
68. A. Zeni and J. Gallas, *Lyapunov exponents for a Duffing oscillator*, Phys. D: Nonlin. Phenom. **89** (1995), 71–82.
69. S. Lenci, *Exact solutions for coupled Duffing oscillators*, Mech. Syst. Signal Process. **165** (2022), 108299.

How to cite this article: V. J. Bevia, J. C. Cortés, and R. J. Villanueva, *Forward uncertainty quantification in random differential equation systems with delta-impulsive terms: Theoretical study and applications*, Math. Meth. Appl. Sci. (2023), 1-21. DOI 10.1002/mma.9226